photonics

MDPI

Article

Research on Nanosecond High-Pulse-Energy Regenerative Amplifier with Adjustable Pulse Duration and Third Harmonic Generation

Mengyao Cheng [1], Hua Wang [2], Wenlong Tian [2], Yizhou Liu [3] and Jiangfeng Zhu [2,*]

[1] School of Artificial Intelligence, Shaanxi Institute of Technology, Xi'an 710300, China; mengyaocheng@126.com
[2] School of Optoelectronic Engineering, Xidian University, Xi'an 710071, China; wanghua@stu.xidian.edu.cn (H.W.); wltian@xidian.edu.cn (W.T.)
[3] School of Information Science and Engineering and Shandong Provincial Key Laboratory of Laser Technology and Application, Shandong University, Qingdao 266237, China; yizhou.liu@sdu.edu.cn
* Correspondence: jfzhu@xidian.edu.cn

Abstract: We reported on a nanosecond regenerative amplified laser with a repetition rate of 1 kHz by employing laser diodes (LDs) with distinct wavelengths as both the seed laser and the pump source and utilizing Nd:YAG as the gain medium. The single-pulse energy was 1.58 mJ and the pulse duration was adjustable, ranging from 1 to 5 ns. Combining two oppositely oriented BBO crystals for second harmonic generation (SHG) and an LBO crystal for third harmonic generation (THG), a 355 nm laser with a single-pulse energy of 257 μJ was attained, corresponding to a THG efficiency of 16.2%.

Keywords: nonlinear optics; frequency conversion; diode-pumped lasers; amplifiers

1. Introduction

Compared to the direct generation of nanosecond infrared lasers from Nd-doped crystals, the high-energy nanosecond ultraviolet laser produced through amplification and third harmonic generation (THG) exhibits superior characteristics, including a higher single-pulse energy, elevated photon energy, and a smaller focal spot size. This laser has been widely applied in research, medical, and industrial fields. Its notable applications include fluorescence lifetime imaging [1], laser-induced breakdown spectroscopy [2], laser surface texturing [3], laser annealing [4–6], the laser processing of ceramics [7–10], and terahertz generation [11]. A particularly compelling application is in the field of radio-photoluminescence (RPL) [12], where there is a pronounced demand for a high-energy nanosecond ultraviolet laser with adjustable pulse duration capabilities.

Traditional nanosecond laser amplifiers typically utilize either Q-switched solid-state lasers [13] or fiber lasers [14,15] as their seed source. Q-switching technology can be categorized into two types: active Q-switching [16] and passive Q-switching [17,18]. High-energy nanosecond lasers often employ passively Q-switched lasers with pulse durations below 10 ns as their seed source. However, these systems lack the ability to adjust their pulse duration flexibly. With the progress in LDs and their driving technologies, using LDs with a center wavelength of 1064 nm and pulse durations below 10 ns as seed sources has become a viable alternative. By this method, the arbitrary adjustment of the regenerative amplifier's output laser pulse duration can be achieved. In addition, using Q-switched lasers as seed sources requires additional components, such as a pump source, attenuation modules, and pulse-selection systems to control pulse energy and repetition rate. This not only increases

check for updates

Received: 14 March 2025
Revised: 2 April 2025
Accepted: 7 April 2025
Published: 8 April 2025

Citation: Cheng, M.; Wang, H.; Tian, W.; Liu, Y.; Zhu, J. Research on Nanosecond High-Pulse-Energy Regenerative Amplifier with Adjustable Pulse Duration and Third Harmonic Generation. *Photonics* **2025**, *12*, 353. https://doi.org/10.3390/photonics12040353

Copyright: © 2025 by the authors. Licensee MDPI, Basel, Switzerland. This article is an open access article distributed under the terms and conditions of the Creative Commons Attribution (CC BY) license (https://creativecommons.org/licenses/by/4.0/).

the overall cost but also compromises system stability. In contrast, nanosecond high-pulse-energy regenerative amplifiers utilizing LDs as seed sources offer significant advantages, including a simple structure, low cost, and continuous pulse duration adjustability. These features make them the optimal choice for achieving high-pulse-energy, pulse-duration-adjustable nanosecond lasers.

Laser amplifiers are broadly classified into two categories: traveling-wave amplifiers and regenerative amplifiers. For nanosecond lasers with repetition rates exceeding 10 kHz, multi-stage traveling-wave amplification can mitigate period-doubling bifurcation [19], achieve higher average power, and generate burst-mode pulse trains. However, for applications requiring lower repetition rates and higher single-pulse energy, particularly when seeding with an LD, regenerative amplifiers are more suitable to amplify the seed to higher energy levels while maintaining excellent beam quality and enabling a more compact system design.

In experiments involving ultraviolet nanosecond laser generation via THG, a two-step process involving initial frequency doubling followed by frequency mixing is often preferred due to the low efficiency of direct THG. In this process, the commonly used nonlinear crystals include LBO [20], BBO [21], and KDP [21], whose physical and optical properties are summarized in Table 1.

Table 1. Parameters of nonlinear crystals.

Crystals	Transmission Range /nm	Damage Threshold [22] /GW·cm^{-2}	$d_{eff\,1}$ [1] /pm·V^{-1}	$d_{eff\,2}$ [2] /pm·V^{-1}	Walk-Off Angle [1] /mrad	Walk-Off Angle [2] /mrad
LBO	160–2600	36.3	0.83 (xy)	0.53 (yz)	7.06 (xy)	9.30 (yz)
BBO	185–2600	18.27	2.01	2.02	55.86	72.33
KDP	177–1700	20	0.26	0.32	28.06	30.12

[1] Under the condition of 1064 nm frequency doubling output at 532 nm. [2] Under the condition of 1064 nm and 532 nm sum frequency output at 355 nm.

From the data presented in the table, BBO crystals can be seen to exhibit the highest nonlinear coefficient, while LBO crystals have the highest damage threshold. Therefore, in nanosecond-pulse THG experiments at lower peak power, it is advantageous to use BBO crystals for SHG and LBO crystals for THG to improve the efficiency and reduce the risk of crystal damage. Additionally, given the pronounced walk-off angle of BBO crystals, using two oppositely oriented BBO crystals for SHG can effectively compensate for the spatial walk-off effect.

For nanosecond ultraviolet lasers, several promising results have demonstrated high conversion efficiency [23]. However, these lasers typically rely on a conventional Q-switched laser, which inherently lack the capability for broad-range, arbitrary-pulse-width tuning. Some studies have used LDs as the seed source for all-fiber regenerative amplifiers [24], but such lasers struggle to achieve a high pulse energy. In this work, we employ an LD as the seed source for an all-solid-state laser regenerative amplifier and THG to produce a high-energy, nanosecond ultraviolet laser with a fully adjustable pulse width.

In summary, a commercial LD with a center wavelength of 1064.3 nm, a peak power of 30 W, and a repetition rate of 1 kHz was used as the seed source for the amplifier. The seed laser's pulse duration was tunable from 1 to 5 ns. For the regenerative amplifier, a fiber-coupled LD served as the pump source, with an Nd:YAG crystal as the gain medium. The regenerative amplification process increased the pulse energy to 1.58 mJ while keeping the pulse duration at 1–5 ns. The amplified laser pulses were focused in order to increase power density, enabling ultraviolet laser generation via two BBO crystals and one LBO crystal. As a result, the system produced a 355 nm laser of 1 ns pulse duration with a single-pulse energy of 257 μJ and a THG efficiency of 16.2%.

2. Experimental Setup

The optical structure of the experimental setup is shown in Figure 1. The experimental setup comprised a seed source, a regenerative amplifier, a THG unit, and an electronic control system.

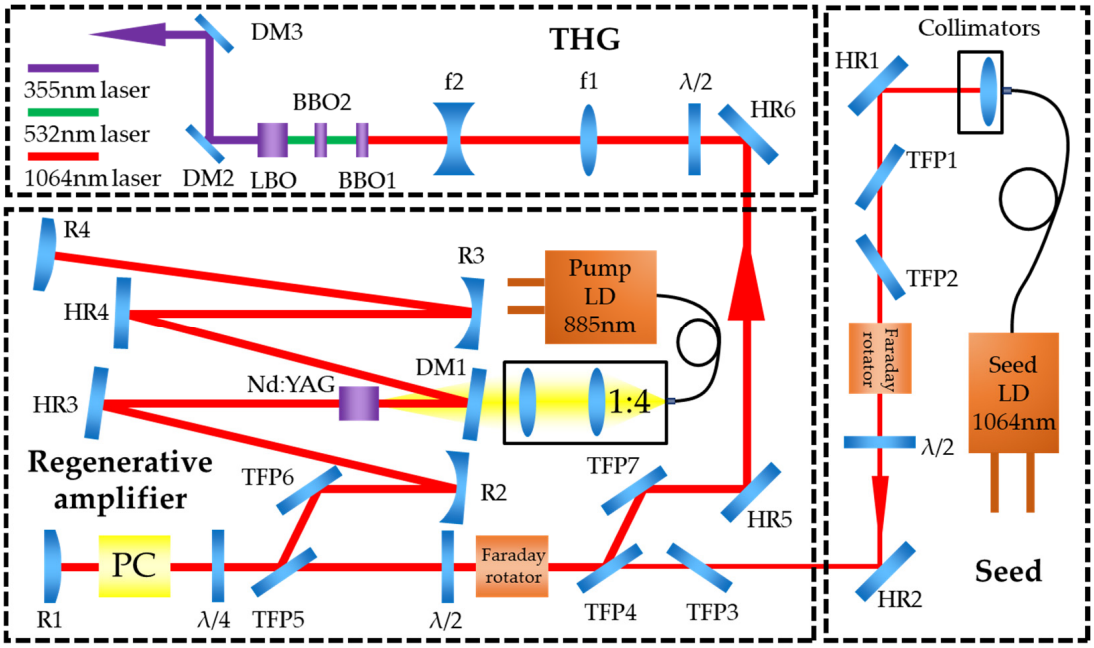


Figure 1. Optical structure of experimental device. (HR, high-reflectivity mirror; DM, dichroic mirror; TFP, thin-film polarizer).

The seed source was a commercial LD with a maximum peak power of 30 W and an adjustable output pulse duration ranging from 1 to 10 ns. By adjusting its operating temperature, the central wavelength could be set at 1064.3 nm, which matched the emission peak of the gain medium in the regenerative amplifier. The repetition rate of the seed LD was adjustable within the range of 0.1–1 kHz, and the seed laser was coupled through a single-mode polarization-maintaining fiber. After using a collimator, the seed laser became horizontally polarized and was injected into two 45° high-reflectivity mirrors (HR1 and HR2). By adjusting the angles of HR1 and HR2, the seed laser could be precisely directed into the regenerative amplifier. Additionally, an isolator composed of two thin-film polarizers (TFP1 and TFP2), a Faraday rotator, and a half-wave plate (λ/2) was inserted between HR1 and HR2 to prevent laser feedback in the regenerative amplifier from damaging the seed source. After the first isolator, the seed laser passed through a second isolator consisting of TFP3, TFP4, a Faraday rotator, and a λ/2 plate, maintaining its horizontal polarization. Subsequently, the laser was transmitted through TFP5 and entered the regenerative amplifier. The regenerative amplifier utilized a fiber-coupled LD with a central wavelength of 885 nm as its pump source. This pump source had a maximum output power of 70 W and used a coupling fiber with a 200 μm core diameter. The pump beam delivered from the fiber was focused into the laser gain medium by a coupling system with magnification of 1 and a dichroic mirror (DM1) with both anti-reflection coating at 885 nm and high-reflectance coating at 1064 nm. The focused beam waist in the gain medium was about 800 μm. To mitigate excessive thermal effects in the gain medium that could degrade amplification efficiency, the pump source was operated in a pulsed mode synchronized with the regenerative amplifier, featuring a 230 μs pulse duration. The regenerative amplifier employed a Nd:YAG crystal (16 mm length, 4 × 4 mm^2 cross-section) with a 0.15-at.% Nd^{3+} doping concentration as the gain medium. For thermal management,

the crystal was encapsulated in indium foil and secured in a gold-plated copper heat sink with water-cooling. To suppress Fabry–Perot etalon effects, all of the crystal's surfaces were deposited with anti-reflection coatings optimized for both 885 nm and 1064 nm, and the crystal was fabricated with a 2° wedge angle. The regenerative amplifier had a total cavity length of 1236 mm, and the symmetric confocal cavity was formed by two concave mirrors, R2 and R3, each with a curvature radius of 900 mm. The end mirrors on both sides of the amplifier were convex mirrors, R1 and R4, with curvature radii of −600 mm. The distances from R2 to the crystal and from R3 to the crystal were both 350 mm. Similarly, the separation between R1 and R2, and between R3 and R4, was 260 mm. To achieve a compact optical layout, plane mirrors HR3 and HR4 were inserted into the cavity to fold the optical path. Using ABCD matrix calculations, the laser beam diameter at the crystal was set to be approximately 1 mm, ensuring excellent mode matching with the 800 μm pump beam. To enable injection and cavity dumping in the regenerative amplifier, a Pockels cell (PC) with a 4 mm aperture and a $\lambda/4$ waveplate were inserted between TFP5 and R1. Additionally, TFP6 was placed between TFP5 and R2 to optimize the optical path. After amplification, the laser exited through TFP5 and passed through a $\lambda/2$ waveplate and a polarizer, where its polarization direction was rotated to the vertical direction. The beam was then reflected by TFP7 and a 45° high-reflectivity mirror (HR5) before entering the THG unit.

In the THG unit, the amplified laser was first reflected by a 45° high-reflectivity mirror (HR6). A $\lambda/2$ waveplate ($\lambda/2$ 3) was inserted after HR6, which allowed us to adjust the incident laser's polarization to achieve a higher conversion efficiency. Due to the large beam diameter and divergence of the amplified laser, a pair of lenses (f1 and f2) were used to reduce the beam size and collimate it after entering the THG unit. This improved the power density and enhanced the conversion efficiency. The focal lengths of f1 and f2 were 150 mm and −50 mm, respectively, and the distance between f1 and f2 was approximately 100 mm. The frequency doubling utilized two BBO crystals placed in opposite directions to compensate for the walk-off effect, as illustrated in Figure 2. Both BBO crystals had a length of 6 mm and a cross-sectional area of 4×4 mm^2, with cutting angles of $\theta = 22.8°$ and $\varphi = 0°$. The crystals were coated on both sides with dielectric films highly transparent to both 1064 nm and 532 nm lasers. For sum frequency generation, a single LBO crystal was used, which was 10 mm in length with a cross-sectional area of 4×4 mm^2 and cutting angles of $\theta = 44.2°$ and $\varphi = 90°$. One side of the LBO crystal was coated with a dielectric film highly transparent to both 1064 nm and 532 nm lasers, and the other side was coated with a dielectric film transparent to 1064 nm, 532 nm, and 355 nm lasers. To achieve precise temperature control of the nonlinear crystals, both crystals were encapsulated in indium foil and secured in a gold-plated copper heat sink with thermoelectric coolers (TECs). The other side of each TEC was cooled by a water-cooled housing. The two BBO crystals shared one set of heat sinks and TECs, while the LBO crystal used another set, allowing for independent temperature controlling. The temperature control range was from 10 °C to 50 °C. After the nonlinear crystals, the laser was reflected by two 45° dichroic mirrors (DM2 and DM3) and then exited through a window plate. Both sides of DM2 and DM3 were coated with dielectric films that highly reflect 355 nm lasers and transmit both 532 nm and 1064 nm lasers, ensuring a pure 355 nm laser output. The window plate was an uncoated fused silica glass plate, positioned at the Brewster angle to achieve high transmission efficiency. Additionally, the window plate featured a sealed design to prevent the contamination of the nonlinear crystals by external air and dust.

To enhance the stability of the laser system, the regenerative amplifier and the THG unit were placed inside a sealed aluminum housing. The housing had a footprint of 570×375 mm^2 and a height of 150 mm. To prevent damage to the nonlinear crystals, the regenerative amplifier and THG stages were isolated by the housing, while the THG cavity

was equipped with replaceable desiccant and specially engineered low-outgassing cables. Next, the seed laser entered the housing through a sidewall-mounted collimator, was amplified by the regenerative amplifier, and was frequency-tripled by the THG unit before exiting through a window plate. The aluminum housing was cooled by circulating water maintained at 24 °C to ensure stable thermal conditions. Heat-generating components, such as the gain medium of the regenerative amplifier, the pump LD, and the TECs for the temperature control of the nonlinear crystals, were all cooled through the housing.

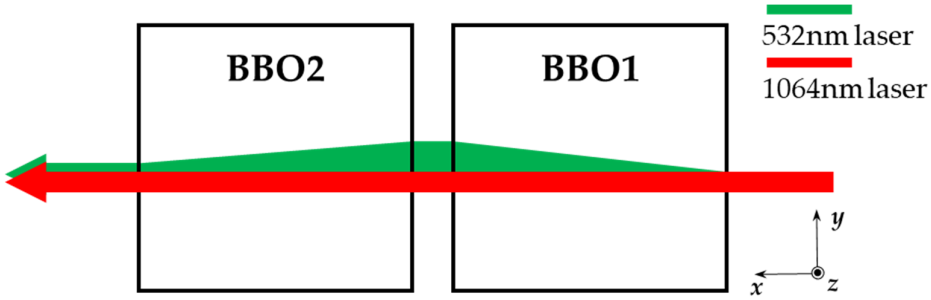


Figure 2. Schematic diagram of space walk-off and compensation for double BBO crystals.

3. Experimental Results

In the laser system, the pulse duration of the seed source LD could be adjusted within the range of 1–10 ns. However, due to the regenerative amplifier cavity length being only 1236 mm, it could only support a maximum pulse duration of 5 ns. Initially, the pulse duration of the seed source was set to 1 ns, and the peak power of the seed pulse output by the seed source reached 30 W, with a repetition frequency of 1 kHz. With the seed source LD's peak power remaining constant, the single-pulse energy scaled proportionally with pulse width. Specifically, at a seed pulse width of 1 ns, the minimum single-pulse energy was 30 nJ, while at a 5 ns pulse width, it increased to 150 nJ. Simultaneously, the seed source also output a synchronization signal identical to the seed pulse to synchronize with the regenerative amplifier.

During the process of adjusting the regenerative amplifier, we first used the seed laser to adjust all the cavity mirrors until the beam could retro-reflect precisely at both end mirrors (R1 and R4 in Figure 1). And the Nd:YAG crystal was intentionally tilted slightly in the horizontal plane to prevent parasitic lasing. Finally, after blocking the seed laser, we carefully adjusted the λ/4 waveplate to achieve quasi-continuous output. At this stage, the pump source operated at a repetition frequency of 1 kHz with a pulse duration of 230 μs, corresponding to a duty cycle of 23%. By meticulously optimizing parameters such as the end mirror angle and the pump coupling distance, and measuring the output laser power with a power meter, we achieved a quasi-continuous output power of 2.17 W at a maximum current of 7.5 A in the pump source LD. Subsequently, we activated the Pockels cell and fine-tuned the λ/4 waveplate. Through the careful adjustment of the Pockels cell voltage, the delay between the Pockels cell and the pump source, the Pockels cell gate width, and the λ/4 waveplate angle, a Q-switched output with a maximum output power of 1.63 W at 7.5 A was achieved. Finally, the seed source was injected into the regenerative amplifier. By precisely adjusting the injection direction of the seed source, the delay between the seed source and the Pockels cell, and the Pockels cell gate width, we achieved a regenerative amplification output power of 1.58 W at the same current of 7.5 A. The output powers under quasi-continuous, Q-switched, and regenerative amplification conditions are summarized in the Table 2:

Table 2. Output power under quasi-continuous, Q-switched, and regenerative amplified conditions.

Current of Pump Source LD/A	Quasi-Continuous Output Power/W	Q-Switched Power/W	Regenerative Amplified Output Power/W
4.5	0.35	0	0
5	0.62	0	0
5.5	0.89	0	0
6	1.20	0.34	0.15
6.5	1.54	1.02	0.78
7	1.87	1.46	1.33
7.5 [1]	2.17	1.63	1.58

[1] The peak power of the pump source at a current of 7.5 A was 50 W.

To prevent potential damage to the nonlinear crystals in the THG unit caused by excessive power, we ultimately conducted subsequent experiments at a pump current of 7.5 A. Under these conditions, the peak power of the pump source was approximately 50 W, the gate width of the Pockels cell was 341 ns, and the output power of the regenerative amplifier was 1.58 W, with a repetition rate of 1 kHz, corresponding to a single-pulse energy of 1.58 mJ. A photodiode and an oscilloscope were used to measure the regenerative amplification pulse buildup sequence and the output laser waveform by detecting the leakage laser from the cavity mirror and the output laser of the regenerative amplifier, respectively. The results are illustrated in Figure 3 below:

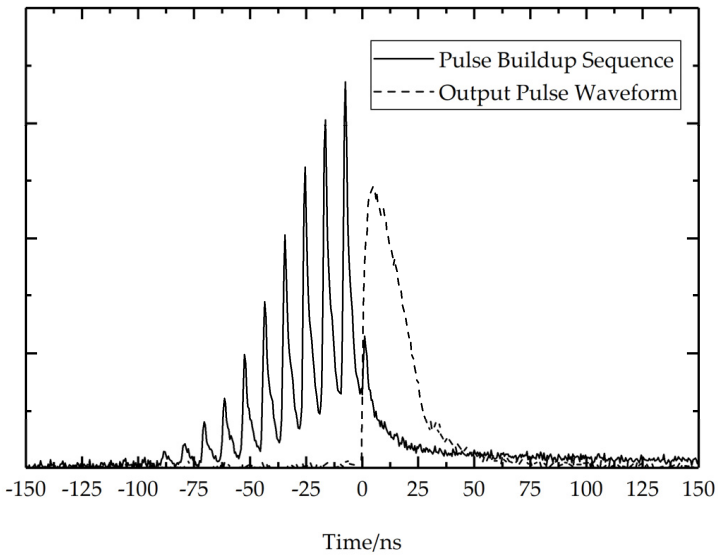


Figure 3. Pulse buildup waveform and output pulse waveform of regenerative amplifier.

Due to the limited bandwidth of the photodiode and oscilloscope we employed, we were unable to accurately measure the pulse duration of the output laser from the regenerative amplifier. We also measured the output power and pulse buildup waveforms of the regenerative amplifier at different pulse durations. It was found that within the seed source pulse duration range of 1–5 ns, the output power and pulse buildup waveforms of the regenerative amplifier did not exhibit significant changes. Additionally, we used a CCD camera to measure the output beam profile of the regenerative amplifier. The measurements revealed that the long-axis diameter of the output beam was 2.26 mm and the short-axis diameter was 2.16 mm, corresponding to a beam roundness of 96%. An image of the output beam profile is shown in Figure 4:

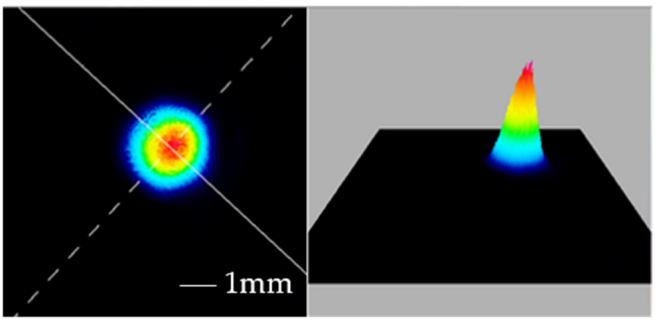


Figure 4. Output laser spot of regenerative amplifier.

In the THG process, due to the large and divergent beam output from the regenerative amplifier, a pair of lenses with focal lengths of f = 150 mm and f = −50 mm were employed to reduce and collimate the beam. Subsequently, by meticulously adjusting parameters such as the incident direction and polarization direction of the fundamental laser, the spacing between the lenses, and the angles and temperatures of the nonlinear crystals, an ultraviolet laser with a single-pulse energy of 257 μJ was achieved under the conditions of a 1.58 mJ single-pulse energy, 1 ns pulse duration, and 1 kHz repetition rate of the infrared laser. The corresponding THG efficiency was 16.2%. At this point, the temperatures of the BBO crystals and LBO crystal were 24.0 °C and 45.8 °C, respectively. During the adjustment process, it was also found that the temperature of the LBO crystal had a significant impact on the efficiency, whereas the temperature of the BBO crystals had a relatively minor effect. This is because the LBO crystal had a higher thermal birefringence coefficient compared to the BBO crystal [21], along with a smaller nonlinear optical coefficient, making its phase-matching conditions more sensitive to temperature variations. The spectrum of the ultraviolet laser, measured using a spectrometer, is shown in Figure 5:

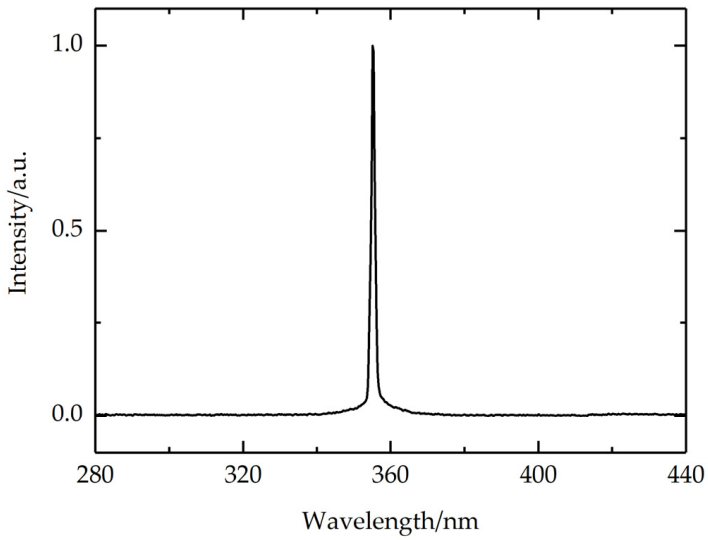


Figure 5. Spectrum of ultraviolet laser.

We also tested the THG efficiency at different pulse durations, with the highest efficiency of 16.2% being at 1 ns and the lowest of 4.68% at 5 ns. This is because the peak power density of the laser is higher at shorter pulse durations, leading to a higher THG efficiency. The variation in THG efficiency at different pulse durations also indirectly demonstrated that using an LD as a seed source enables the adjustment of the output laser pulse duration from the amplifier. The curve of the ultraviolet laser output power at different pulse durations is shown in Figure 6:

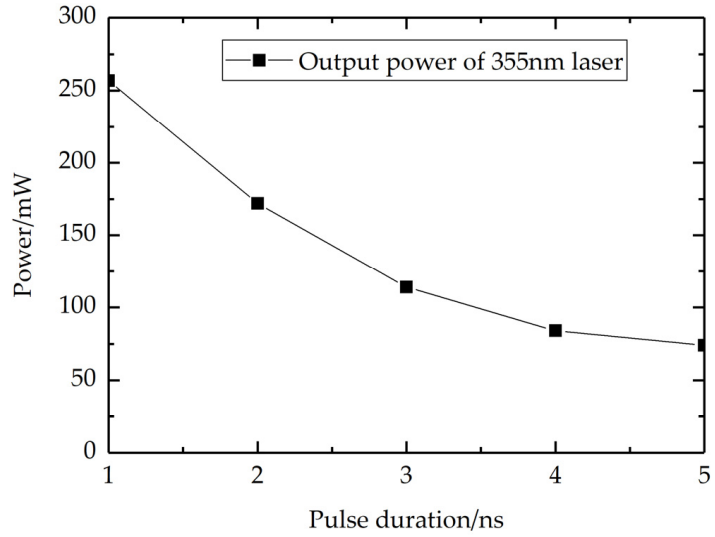


Figure 6. Output power of ultraviolet laser at different pulse durations.

Finally, after sealing the housing, we measured the power stability of the laser over a period of one hour. The root mean square (RMS) error of the average power was less than 1%, indicating that the laser exhibits excellent overall stability and can operate reliably in the long term as a commercial laser. The power stability curve is shown in Figure 7:

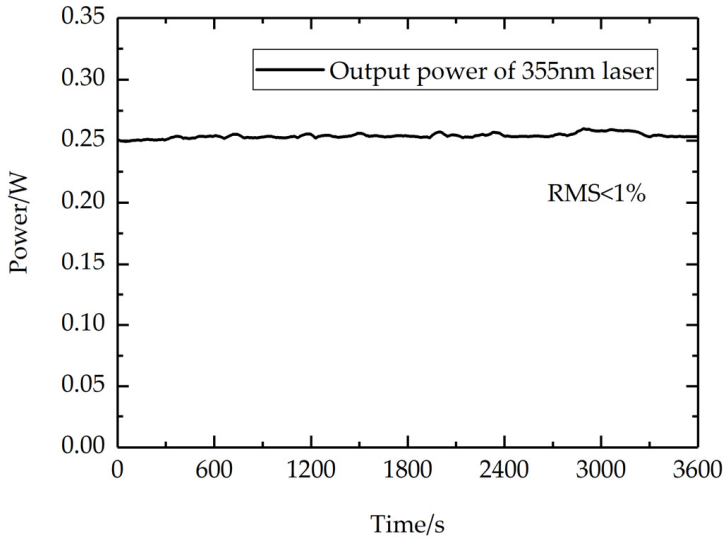


Figure 7. Stability of ultraviolet laser output power.

4. Summary and Outlook

In summary, using LDs as the seed and pump sources, we demonstrated a Nd:YAG nanosecond regenerative amplifier with a repetition rate of 1 kHz, a single-pulse energy of 1.58 mJ, and an adjustable pulse duration ranging from 1 to 5 ns. By employing two counter-positioned BBO crystals and one LBO crystal for THG, we obtained a maximum output of 257 μJ at 355 nm with a pulse duration of 1 ns, corresponding to a THG efficiency of 16.2%, which is notably high for nanosecond ultraviolet lasers [23,25]. The entire laser system was enclosed in a sealed aluminum box measuring 570 × 375 × 150 mm^3, with a power stability of less than 1% over one hour. This nanosecond 355 nm laser with tunable pulse duration and high-power energy can be widely used in fluorescence lifetime imaging, laser-induced breakdown spectroscopy, laser surface texturing, laser annealing, the laser processing of ceramics, and terahertz generation. In future work, we plan to increase the

infrared laser output power by adding a traveling-wave amplification stage, and further improve the THG efficiency by optimizing the nonlinear crystal parameters.

Author Contributions: Conceptualization, M.C. and J.Z.; methodology, W.T.; software, M.C.; validation, M.C. and H.W.; formal analysis, W.T.; investigation, M.C.; resources, J.Z.; data curation, M.C.; writing—original draft preparation, M.C.; writing—review and editing, W.T.; visualization, W.T.; supervision, J.Z.; project administration, J.Z.; funding acquisition, Y.L. All authors have read and agreed to the published version of the manuscript.

Funding: This research was funded by the Shaanxi Provincial Department of Education Key Scientific Research Program Projects (24JR017) and the Annual Scientific Research Plan of Shaanxi Institute of Technology (Pt24-01).

Institutional Review Board Statement: Not applicable.

Informed Consent Statement: Not applicable.

Data Availability Statement: The data presented in this study are available on request from the corresponding author. The data are not publicly available due to the fact that the data also form part of an ongoing study.

Conflicts of Interest: The funders had no role in the design of the study; in the collection, analyses, or interpretation of data; in the writing of the manuscript; or in the decision to publish the results.

References

1. Awasthi, K.; Nakabayashi, T.; Ohta, N. Application of Nanosecond Pulsed Electric Fields into HeLa Cells Expressing Enhanced Green Fluorescent Protein and Fluorescence Lifetime Microscopy. *J. Phys. Chem. B* **2012**, *116*, 11159–11165. [CrossRef] [PubMed]
2. Zhang, D.; Zhang, Z.; Zhang, M.; Feng, Z.; Gu, T.; Shen, K.; Li, S.; Hou, J.; Zhu, J. Portable nanosecond laser for handheld laser-induced breakdown spectroscopy instruments. *Opt. Eng.* **2023**, *62*, 036102. [CrossRef]
3. Bakhtiyari, A.N.; Yadav, A.; Wu, Y.; Zheng, H. Enhancing wettability of sapphire (Al_2O_3) substrate through laser surface texturing. *Mater. Lett.* **2024**, *355*, 135506. [CrossRef]
4. Park, S.Y.; Choi, Y.; Seo, Y.H.; Kim, H.; Lee, D.H.; Truong, P.L.; Jeon, Y.; Yoo, H.; Kwon, S.J.; Lee, D.; et al. 355 nm Nanosecond Ultraviolet Pulsed Laser Annealing Effects on Amorphous In-Ga-ZnO Thin Film Transistors. *Micromachines* **2024**, *15*, 103. [CrossRef]
5. Wang, H.; Zhang, F.; Wang, C.; Duan, J. Broadband antireflective subwavelength structures for infrared detection. *Opt. Laser Technol.* **2022**, *149*, 107931. [CrossRef]
6. Ding, Y.; Liu, L.; Wang, C.; Li, C.; Lin, N.; Niu, S.; Han, Z.; Duan, J. Bioinspired Near-Full Transmittance MgF_2 Window for Infrared Detection in Extremely Complex Environments. *ACS Appl. Mater. Interfaces* **2023**, *15*, 30985–30997. [CrossRef]
7. Jia, X.; Lin, J.; Li, Z.; Wang, C.; Li, K.; Wang, C.; Duan, J. Continuous wave laser ablation of alumina ceramics under long focusing condition. *J. Manuf. Process.* **2025**, *134*, 530–546. [CrossRef]
8. Li, Z.; Lin, J.; Jia, X.; Li, X.; Li, K.; Wang, C.; Sun, K.; Ma, Z.; Duan, J. High efficiency femtosecond laser ablation of alumina ceramics under the filament induced plasma shock wave. *Ceram. Int.* **2024**, *50*, 47472–47484. [CrossRef]
9. Jia, X.; Luo, J.; Guo, C.; Li, Z.; Ma, Z.; Xiang, Y.; Yi, Z.; Li, K.; Wang, C.; Li, X.; et al. High-energy continuous wave laser ablation of alumina ceramic. *J. Mater. Res. Technol.* **2023**, *27*, 5389–5403. [CrossRef]
10. Jia, X.; Li, Z.; Wang, C.; Li, K.; Zhang, L.; Ji'an, D. Study of the dynamics of material removal processes in combined pulse laser drilling of alumina ceramic. *Opt. Laser Technol.* **2023**, *160*, 109053. [CrossRef]
11. Hayashi, S.; Shibuya, T.; Sakai, H.; Taira, T.; Otani, C.; Ogawa, Y.; Kawase, K. Tunability enhancement of a terahertz-wave parametric generator pumped by a microchip Nd: YAG laser. *Appl. Opt.* **2009**, *48*, 2899–2902. [CrossRef] [PubMed]
12. Maki, D.; Sato, F.; Kato, Y.; Yamamoto, T.; Iida, T. Improvement of a dose reading system for radiophotoluminescence glass dosimeters. *Radioisotopes* **2011**, *60*, 55–61. [CrossRef]
13. Li, B.; Sun, B.; Mu, H. High-efficiency generation of 355 nm radiation by a diode-end-pumped passively Q-switched Nd:YAG/Nd:YVO_4 laser. *Appl. Opt.* **2016**, *55*, 2474–2477. [CrossRef] [PubMed]
14. Yang, A. Experimental Demonstration of a Ring-Cavity Q-Switched Fiber Regenerative Amplifier. *Jpn. J. Appl. Phys.* **2006**, *45*, L673. [CrossRef]
15. Peng, Z.; Shi, Y.; Bu, X.; Hong, C.; Li, H.; Xu, Y.; Wang, P. 21 W, 105 μJ Regenerative Amplifier Based on Yb:YAG SCF and NALM Fiber Oscillator. *IEEE Photonics Technol. Lett.* **2020**, *32*, 333–336. [CrossRef]

16. Li, Y.; Tu, W.; Wang, B.; Zong, N.; Yang, F.; Zhang, F.; Zhang, S.; Wang, Z.; Peng, Q.; Cui, D.; et al. High-Power Narrow-Linewidth Q-Switched TEM00 Mode 355-nm Laser. *IEEE Photonics J.* **2018**, *10*, 1–9. [CrossRef]
17. Huang, Y.J.; Huang, Y.P.; Chiang, P.Y.; Liang, H.C.; Su, K.W.; Chen, Y.F. High-power passively Q-switched Nd:YVO4 UV laser at 355 nm. *Appl. Phys. B* **2011**, *106*, 893–898. [CrossRef]
18. Sakai, H.; Kan, H.; Taira, T. >1 MW peak power single-mode high-brightness passively Q-switched Nd3+: YAG microchip laser. *Opt. Express* **2008**, *16*, 19891–19899. [CrossRef]
19. Dörring, J.; Killi, A.; Morgner, U.; Lang, A.; Lederer, M.; Kopf, D. Period doubling and deterministic chaos in continuously pumped regenerative amplifiers. *Opt. Express* **2004**, *12*, 1759–1768. [CrossRef]
20. Zhu, P.; Li, D.; Liu, Q.; Chen, J.; Fu, S.; Shi, P.; Du, K.; Loosen, P. 39.1 μJ picosecond ultraviolet pulses at 355 nm with 1 MHz repeat rate. *Opt. Lett.* **2013**, *38*, 4716–4718. [CrossRef]
21. Borsutzky, A.; Brünger, R.; Huang, C.; Wallenstein, R. Harmonic and sum-frequency generation of pulsed laser radiation in BBO, LBO, and KD* P. *Appl. Phys. B* **1991**, *52*, 55–62. [CrossRef]
22. Yoshida, H.; Fujita, H.; Nakatsuka, M.; Yoshimura, M.; Sasaki, T.; Kamimura, T.; Yoshida, K. Dependences of Laser-Induced Bulk Damage Threshold and Crack Patterns in Several Nonlinear Crystals on Irradiation Direction. *Jpn. J. Appl. Phys.* **2006**, *45*, 766–769. [CrossRef]
23. Zhang, B.T.; Huang, H.T.; Yang, J.F.; He, J.L.; Zuo, C.H.; Xu, J.L.; Yang, X.Q.; Zhao, S. Generation of 7.8W at 355nm from an efficient and compact intracavity frequency-tripled Nd:YAG laser. *Opt. Commun.* **2010**, *283*, 2369–2372. [CrossRef]
24. Wang, X.; Wang, B.; Guo, S.; Cheng, W. Stable and compact nanosecond pulse seed source with diode laser driven by a high-speed circuit and a temperature control circuit. *Optik* **2019**, *179*, 1123–1128. [CrossRef]
25. Wang, G.; Liu, J.; Liu, S.; Liu, M.; Liu, S.; Li, L. Short pulse duration of a 355-nm laser by extracavity sum-frequency mixing with a LiB_3O_5 (LBO) crystal. *Laser Phys. Lett.* **2008**, *5*, 506–509. [CrossRef]

Disclaimer/Publisher's Note: The statements, opinions and data contained in all publications are solely those of the individual author(s) and contributor(s) and not of MDPI and/or the editor(s). MDPI and/or the editor(s) disclaim responsibility for any injury to people or property resulting from any ideas, methods, instructions or products referred to in the content.